ACS Catalysis

Research Article

pubs.acs.org/acscatalysis

Efficient H_2 Evolution Coupled with Oxidative Refining of Alcohols via A Hierarchically Porous Nickel Bifunctional Electrocatalyst

Bo You,[†,§] Xuan Liu,[†,§] Xin Liu,[†,‡,§] and Yujie Sun*[,†]

[†]Department of Chemistry and Biochemistry, Utah State University, Logan, Utah 84322, United States

[‡]Key Laboratory of Comprehensive and Highly Efficient Utilization of Salt Lake Resources, Chinese Academy of Sciences, 18 Xinning Road, Xi'ning, Qinghai 810008, People's Republic of China

Supporting Information

ABSTRACT: Water electrolysis to produce H_2 and O_2 with renewable energy input has been generally viewed as an attractive route to meet future global energy demands. However, the sluggish O_2 evolution reaction usually requires high overpotential and may yield reactive oxygen species (ROS) that can degrade the electrolyzer membrane and hence shorten the device lifetime. In addition, the potential gas crossover may result in an explosive H_2/O_2 mixture and hence safety risks. To address these issues, we herein report a general electrolysis strategy for the simultaneous H_2 production and alcohol oxidative upgrading (e.g., benzyl alcohol, 4-nitrobenzyl alcohol, 4-methylbenzyl alcohol, ethanol, and 5-hydroxymethylfurfural), in which the thermodynamics of the latter is much easier than that of water oxidation. A facile and environmentally friendly template-free electrodeposition was used to obtain a 3D hierarchically porous nickel-based electrocatalyst (hp-Ni) for such an integrated electrolysis, requiring a voltage of ~220 mV smaller than that of water splitting to achieve 50 mA cm^{-2} together with robust stability, high Faradaic efficiencies, and no formation of ROS, as well as production of valuable products at both the cathode (H_2) and anode (alcohol oxidation products). More importantly, we demonstrated that these diverse alcohol oxidations over hp-Ni exhibited similar onset potentials which were largely determined by the desirable oxidation potential of hp-Ni, irrespective of the different intrinsic thermodynamics of these alcohol oxidation reactions. This result provides a new direction for the rational design of heterogeneous transition-metal-based electrocatalysts with lower oxidation potential for more highly efficient electrocatalytic alcohol oxidation.

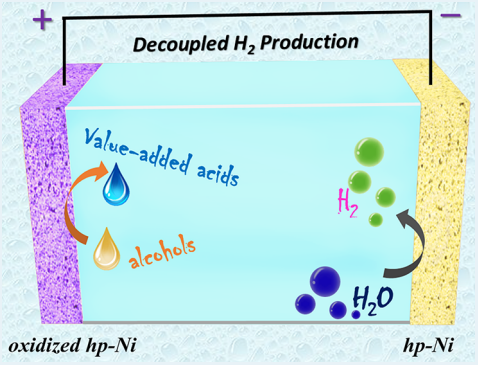

KEYWORDS: *electrocatalysis, alcohol oxidation, hydrogen evolution, water splitting, nickel*

INTRODUCTION

Hydrogen (H_2) generation from water electrolysis driven by renewable energy offers an attractive option to alleviate the impending global energy crisis and associated environmental issues due to the consumption of finite fossil fuels.[1−6] Conventional room-temperature water electrolyzers usually perform under either strongly alkaline or acidic conditions with state of the art noble metal-based catalysts (e.g., Pt, Ir, and Ru). However, the high price and scarcity of these noble-metal catalysts undoubtedly prohibit their large-scale implementation and necessitate the exploration of low-cost alternatives. Recent years have witnessed the emergence of promising transition metal (such as Mo, W, Co, Ni, and Fe) based borides, carbides, nitrides, phosphides, sulfides, and selenides for the H_2 evolution reaction (HER).[2,3,7,8] In addition, transition-metal-based oxides, hydroxides, and (oxy)hydroxide have also been reported with appreciable activities for the O_2 evolution reaction (OER).[9−12] In particular, our group reported the concept of "single bifunctional electrocatalyst for overall water splitting under alkaline solution" based on cobalt−phosphorus-derived (Co−P) films.[13] This bifunctional electrocatalyst strategy was subsequently extended to other transition-metal derivatives and even metal-free nanocarbons by us[13] and other groups.[14−19] However, high overpotentials are still needed to drive water splitting at high current densities.

In addition, traditional water electrolysis produces H_2 and O_2 simultaneously.[20−22] Therefore, potential gas crossover may result in the formation of an explosive H_2/O_2 mixture and hence poses safety issues.[23−26] Meanwhile, the coexistence of H_2, O_2, and catalysts may yield reactive oxygen species (ROS) which shorten the lifetime of the water electrolyzer.[24] Furthermore, the sluggish kinetics of the OER typically restricts the rate of the HER, and the product of OER, O_2, is actually not a highly valuable chemical.[27−31] Within these considerations in mind, researchers have been devoted to exploring alternative strategies to decouple H_2 production from the OER. For instance, a novel method of electron-coupled proton buffer (ECPB) has been introduced to produce H_2 and O_2 at separate times during water splitting.[23−26] However, the associated requisite of noble-metal-based catalysts and three-compartment

Received: March 19, 2017
Revised: May 7, 2017
Published: May 30, 2017

DOI: 10.1021/acscatal.7b00876
ACS Catal. 2017, 7, 4564−4570

configuration complicates device construction and potentially increases the cost.[23−26] More importantly, a high potential is still needed to catalyze the OER, and the possible decomposition and high cost of ECPB may limit its large-scale commercialization.[23−26] In addition, most non-precious-metal OER electrocatalysts cannot survive the strongly acidic environment of the ECPB-containing electrolytes.[32−34]

In order to address the above concerns, we reason that replacing the OER with a thermodynamically more favorable alcohol oxidation would be an appealing option. Integrating decoupled H_2 production from water splitting with alcohol oxidation would not only reduce the voltage requirement to generate H_2 but also avoid the H_2/O_2 mixture issue. Furthermore, such an integrated electrolyzer would also exclude the formation of ROS and thus may lead to a longer device lifetime. In fact, alcohol oxidation reactions play a vital role in converting many petroleum- and biomass-derived feedstocks to value-added chemicals.[27,35] For example, the oxidation products of benzyl alcohol, ethanol, and 5-hydroxymethylfurfural (HMF) are primary building blocks to produce diverse large-scale commodities, polymers, and pharmaceuticals.[35−39] The overall reactions for H_2 production paired with alcohol oxidation under alkaline conditions are depicted in Figure 1.

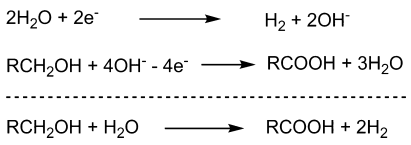

Figure 1. Chemical reactions for integrated H_2 production and alcohol oxidation in alkaline media.

Herein, we report a novel and general strategy of using a 3D hierarchically porous nickel framework (hp-Ni) as a non-precious-metal bifunctional electrocatalyst for H_2 production and oxidative upgrading of various alcohols (e.g., benzyl alcohol, 4-nitrobenzyl alcohol, 4-methylbenzyl alcohol, ethanol, and HMF) under ambient conditions. Since alcohol oxidation occurs at the hp-Ni anode while the HER takes place at the hp-Ni cathode, no O_2 is generated and hence the issues of H_2/O_2 mixing and ROS no longer exist. Furthermore, due to the superior electrocatalytic performance of hp-Ni for alcohol oxidation relative to the OER, the cell voltage of our hp-Ni-based two-electrode electrolyzer at a benchmark current density (50 mA cm^{-2}) was reduced by ∼220 mV, in comparison with that of water electrolysis. Additionally, high Faradaic efficiencies were obtained for both H_2 production and alcohol oxidation, together with robust durability. In comparison with previous reports for electrocatalyst synthesis,[15,16,29,31] the preparation of hp-Ni in the present work is much more facile and environmentally friendly and avoids high-temperature treatment (∼300 °C) and toxic chemical reagents (e.g., sodium hypophosphite monohydrate, sulfur, ammonia gas, etc.). Moreover, the relationship between the electronic effect of alcohols on their oxidation behaviors over hp-Ni catalyst was also investigated, which provides guidance in developing more competent electrocatalysts for alcohol oxidation coupled with H_2 production. Overall, the low cost and green preparation for bifunctional electrocatalyst, high-value products at both electrodes, and better energy conversion efficiency render our strategy particularly attractive for renewable energy conversion technologies, which can be applied to couple the HER with many other organic oxidation reactions.

EXPERIMENTAL SECTION

Chemicals. Benzyl alcohol (BA), benzoic acid, benzaldehyde, 4-nitrobenzyl alcohol (NBA) and 4-methylbenzyl alcohol (MBA) were used as received from Sigma-Aldrich. Ethanol was used as received from Decon Laboratories. 5-Hydroxymethylfurfural (HMF) and 2,5-furandicarboxylic acid (FDCA) were purchased from Alfa Aesar and Chem-Impex International Inc., respectively. 2,5-Diformylfuran (DFF) and 2-formyl-5-furancarboxylic acid (FFCA) were purchased from Ark Pharm, Inc. 5-Hydroxymethyl-2-furancarboxylic acid (HMFCA) was purchased from Asta Tech. Potassium hydroxide was used as received from Alfa Aesar. Ammonium chloride was purchased from Avantor. Nickel chloride was purchased from Fisher, and nickel foam with purity >99.99% was purchased from MTI. The anion exchange membrane (Fumasep FAA-3-PK-130) was purchased from Fuel Cell Store. All chemicals were used as received without purification. Deionized water (18 MΩ cm) from a Barnstead E-Pure system was used in all experiments.

Synthesis of hp-Ni Electrocatalyst. The hp-Ni bifunctional electrocatalyst was prepared by a facile template-free cathodic electrodeposition of 3D hierarchically porous Ni microspheres on a nickel foam (hp-Ni). Typically, the electrodeposition was performed under a standard two-electrode configuration at room temperature with an electrolyte consisting of 2.0 M NH_4Cl and 0.1 M $NiCl_2$. A piece of commercial nickel foam with a size of 0.5 cm × 0.5 cm was employed as the working electrode and a Pt wire as the auxiliary electrode. The galvanostatic electrodeposition was carried out at −3.0 A cm^{-2} for 500 s to obtain hp-Ni samples with a mass loading of ∼75 mg cm^{-2}.

Physical Methods. Scanning electron microscopy and element mapping were performed on a FEI QUANTA FEG 650 instrument (FEI, USA) at the Microscopy Core Facility of Utah State University. X-ray diffraction patterns were obtained by a Rigaku MinifexII Desktop X-ray diffractometer. The X-ray photoelectron spectroscopy (XPS) analyses were conducted on a Kratos Axis Ultra instrument (Chestnut Ridge, NY) at the Surface Analysis Laboratory, University of Utah Nanofab. XPS data were analyzed via CASA XPS software, and energy corrections on high-resolution scans were calibrated by referencing the C 1s peak of adventitious carbon to 284.5 eV.

Electrocatalytic Measurements. Electrochemical HER, OER, and alcohol oxidation measurements were performed with a Gamry Interface 1000 electrochemical workstation under a three-electrode configuration. The as-prepared hp-Ni was directly used as the working electrode, a Ag/AgCl (saturated KCl) electrode as the reference electrode, and a carbon rod as the counter electrode. All of the reported potentials were quoted with respect to the reversible hydrogen electrode (RHE) through $E_{RHE} = E_{Ag/AgCl} + 0.059 \times pH + 0.197$ V, and overpotential for the OER (η) was calculated from $\eta = E_{RHE} - 1.23$ V. The electrochemical HER, OER, and alcohol oxidation experiments were conducted in 10 mL of a 1.0 M KOH solution in the presence or absence of 10 mM organic substrates. H_2- and O_2-saturated electrolytes were used for HER and OER measurements, respectively. For two-electrode electrolysis, the two hp-Ni samples were employed as bifunctional catalyst electrodes for both the anode and cathode. The entire potential range was scanned at a scan rate of 2 mV s^{-1}. *iR* (current times internal resistance) compensation was

DOI: 10.1021/acscatal.7b00876
ACS Catal. 2017, 7, 4564−4570

employed in all the electrochemical measurements to adjust the voltage drop between the reference and working electrodes by the Gamry Framework Data Acquisition Software 6.11. The stability tests of hp-Ni for BA and HMF oxidation were evaluated by chronoamperometry at 1.423 V vs RHE in 10 mL of 1.0 M KOH containing 10 mM of the corresponding organic substrates for five consecutive cycles.

Product Quantification. To analyze the products of BA and HMF oxidation quantitatively and calculate the corresponding Faradaic efficiencies, 10 μL aliquots of the electrolyte solution during chronoamperometry testing were collected periodically from the electrolysis solution and diluted with 490 μL of water, which were then analyzed using HPLC (Shimadzu Prominence LC-2030C system equipped with an ultraviolet−visible detector and a 4.6 mm × 150 mm Shim-pack GWS 5 μm C18 column). The wavelengths of the detector were set at 230 nm for benzoic acid, 254 nm for benzyl alcohol and benzaldehyde, and 265 nm for HMF and its corresponding products. An eluent mixture of 5 mM ammonium formate aqueous solution (A) and methanol (B) was used. The HPLC analysis was conducted for the BA oxidation products by A/B (v/v 4/6), while HMF oxidation products were determined by A/B (v/v 7/3) within 10 min at a flow rate of 0.5 mL min^{-1}. The qualitative and quantitative analyses of reactants and products were conducted on the basis of the corresponding calibration curves by applying standard solutions with known concentrations. The ^{1}H NMR spectra were obtained on a Bruker Avance III HD Ascend 500 MHz NMR.

A SRI 8610C gas chromatograph with a Molecular Sieve 13 packed column, a HayesSep D packed column, and a thermal conductivity detector was used to quantify the generated H_2 during electrolysis. The oven temperature was set at 80 °C, and argon was used as the carrier gas.

RESULTS AND DISCUSSION

The hp-Ni electrocatalyst with 3D open porosity was prepared by a facile one-step self-template electrodeposition of a metallic Ni framework on commercial Ni foam at −3.0 A cm^{-2} for 500 s. The concomitant formation of H_2 bubbles during electrodeposition functioned as templates for the resulting porosity.[22] The successful formation of metallic Ni for hp-Ni was verified by the corresponding X-ray diffraction (XRD) pattern (Figure 2a). A scanning electron microscopy (SEM) image (Figure 2b) indicated the 3D hierarchically macroporous feature of hp-Ni with pore sizes of several hundred micrometers, inherited from the pristine Ni foam (Figure S1a in the Supporting Information). In addition, there were abundant smaller macropores with diameters of approximately 10 μm on the interconnected macropore walls of hp-Ni (Figure 2b), distinctively different from the featureless surface of a pristine Ni foam (Figure S1b). A closer inspection of the smaller macropores at higher magnification showed a 3D porous structure and the presence of stacked Ni nanospheres with a smooth surface (Figure 2c). These distinct differences clearly confirmed the successful electrodeposition of porous Ni microspheres on Ni foam. Elemental mapping images (Figure S2 in the Supporting Information) revealed the presence of abundant Ni, plus a small amount of O due to slight surface oxidation in air. XPS analysis further confirmed the presence of metallic Ni and O (Figure S3 in the Supporting Information), in line with the XRD and elemental mapping results. It is expected that these hierarchically porous structures with 3D configuration can facilitate substrate transport and gas diffusion

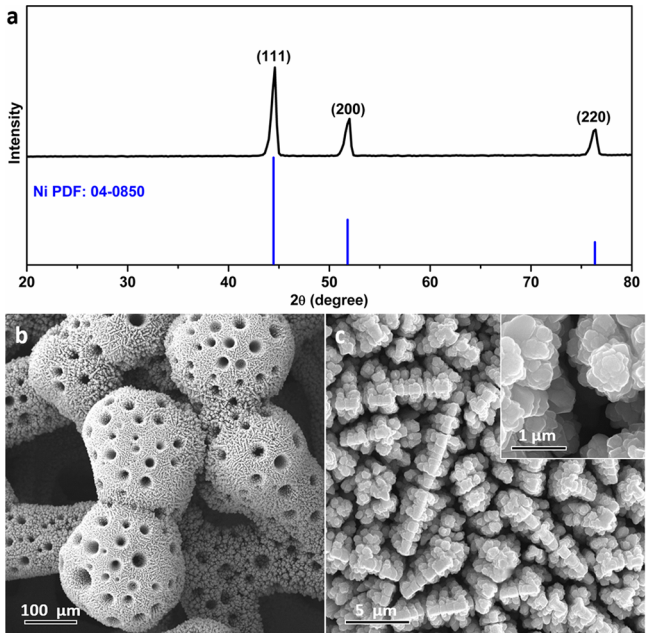

Figure 2. (a) XRD pattern of hp-Ni and the standard pattern of metallic Ni. (b, c) SEM images of hp-Ni at different magnifications.

to boost the utilization efficiency of active sites, which are beneficial for electrocatalytic applications.[22,34,40−44]

Alcohol oxidation is an important reaction in the chemical industry, with applications ranging from petroleum chemical refining and biomass utilization to pharmaceutical and fine chemical synthesis.[27,35] The conventional methods for alcohol oxidation typically require stoichiometric chemical oxidants and expensive metal catalysts (such as Au, Pd, and Pt) under harsh conditions (e.g., high pressure and/or elevated temperature);[37] hence, it is of paramount importance to explore greener and lower-cost alternative methods for alcohol oxidation. Electrocatalytic oxidation under ambient conditions is an appealing approach, as the oxidation can be solely performed by electricity without additional chemical oxidants.[28−31,35,39] Herein, we chose benzyl alcohol (BA) as our first candidate to evaluate the electrocatalytic activity of hp-Ni for alcohol oxidation. The target product is benzoic acid. Under alkaline conditions (1.0 M KOH), the oxygen evolution reaction can potentially compete with organic oxidation reactions. Therefore, an ideal electrocatalyst should possess high preference toward BA oxidation rather than oxygen evolution, which guarantees the minimum Faradaic efficiency loss due to water oxidation. Figure 3a shows the linear sweep voltammetry (LSV) curves of BA oxidation and water oxidation catalyzed by hp-Ni in 1.0 M KOH in the presence and absence of 10 mM BA, respectively. In the absence of BA, the onset potential of our hp-Ni was ∼1.51 V vs RHE and high current density beyond 1.55 V vs RHE was observed, implying the OER activity of hp-Ni. After 10 mM BA was added, the hp-Ni exhibited negatively shifted onset potential (∼1.35 V vs RHE) and a large current density within 1.40 V vs RHE, indicating that the oxidation of BA on hp-Ni was significantly easier than the OER. In stark contrast, the pristine nickel foam (NF) exhibited much worse activities for both the OER and BA oxidation reaction (Figure S4 in the Supporting Information), underscoring the positive effect of a 3D hierarchically porous Ni framework deposited on Ni foam for electrocatalysis. Such an improved catalytic performance of hp-Ni in comparison to that of NF is attributed

DOI: 10.1021/acscatal.7b00876
ACS Catal. 2017, 7, 4564−4570

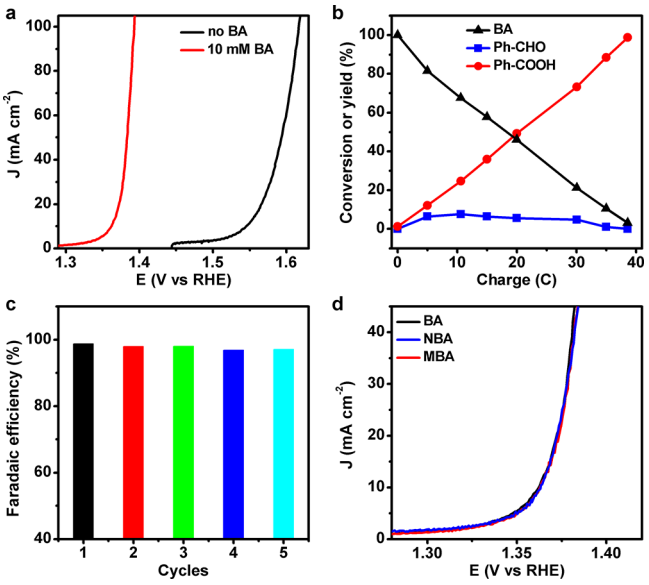

Figure 3. (a) Linear sweep voltammograms of hp-Ni at 2 mV s^{-1} in 1.0 M KOH containing 0 and 10 mM benzyl alcohol (BA). (b) Conversion or yield (%) dependence of BA and its oxidation products on passed charges during electrochemical oxidation at 1.423 V vs RHE in 10 mL of 1.0 M KOH with 10 mM BA (Ph-CHO, benzyl aldehyde; Ph-COOH, benzoic acid). (c) Faradaic efficiencies of benzoic acid production for controlled-potential electrolysis with hp-Ni in 10 mL of 1.0 M KOH with 10 mM BA at 1.423 V vs RHE under five successive cycles. (d) LSV curves of hp-Ni at 2 mV s^{-1} in 1.0 M KOH with 10 mM BA, 4-methylbenzyl alcohol (MBA), or 4-nitrobenzyl alcohol (NBA).

to the synergetic effect of its unique 3D structure, which facilitates gas diffusion and substrate transportation, together with a higher electrochemically active surface area, which will boost the utilization efficiency of active sites (Figure S5 in the Supporting Information).

Next, long-term chronoamperometry utilizing hp-Ni as the electrocatalyst was carried out at 1.423 V vs RHE in 10 mL of 1.0 M KOH containing 10 mM BA. The concentration evolution of BA and its oxidative products (benzyl aldehyde and benzoic acid) during the electrolysis were analyzed by HPLC. Herein, a theoretical charge of ~38 C was needed for the complete oxidation of BA to benzoic acid. As depicted in Figure 3a, no noticeable oxygen evolution could occur at 1.423 V; hence, a high Faradaic efficiency for benzyl alcohol (BA) oxidation was anticipated. The resulting HPLC chromatograms (Figure S6 in the Supporting Information) undoubtedly demonstrated the increase of benzoic acid (Figure S6a) and decrease of BA (Figure S6b) over passed charges, implying the conversion of benzyl alcohol into benzoic acid (Figure 3b). After ~38 C was passed, the peak of BA nearly disappeared (Figure S6b) while the benzoic acid peak reached its maximum intensity (Figure S6a). Eventually, a Faradaic efficiency of 98% was obtained (see the Supporting Information for details of calculations). Note that the intermediate, benzaldehyde (Figure 4a), was also detected during the chronoamperometry experiment but remained at low concentration (Figure S6c).

The stability of hp-Ni for BA oxidation was also estimated by repeating the above constant potential electrolysis using the same hp-Ni catalyst. As exhibited in Figure 3c, the Faradaic efficiencies of benzoic acid production for these five trials were

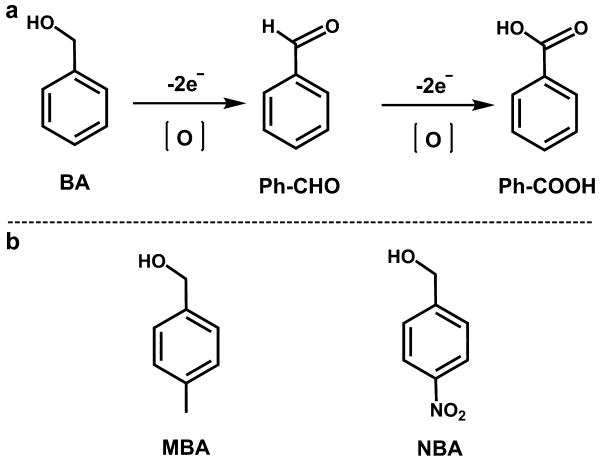

Figure 4. (a) Pathway of benzyl alcohol (BA) oxidation to benzoic acid. (b) Chemical structures of MBA and NBA.

calculated to be 96–98%, unambiguously demonstrating the robust durability of hp-Ni for BA oxidation.

As an initial attempt to investigate the electronic effect on the electrocatalytic activity of hp-Ni for alcohol oxidation, two derivatives of benzyl alcohol with electron-withdrawing (4-nitrobenzyl alcohol, NBA) and -donating (4-methylbenzyl alcohol, MBA) substituents on the benzene ring (Figure 4b) were subjected to similar electrocatalytic oxidation. As shown in Figure 3d, both LSV curves of these two new substrates took off at a quite similar potential in comparison to that of the parent benzyl alcohol. This result implies that the catalytic onset potential of these three alcohol oxidations is primarily determined by the desirable oxidation state of the electrocatalyst, rather than their intrinsic thermodynamics, distinct from the case for many molecular electrocatalysts.[6] Therefore, we anticipate that the optimal solid-state electrocatalysts for alcohol oxidation should require a lower potential to reach their functional oxidation states (high-valence states), which will be pursued in our future studies.

We then employed XRD, SEM, and XPS techniques to probe the structure and composition details of the hp-Ni electrocatalyst after the above stability tests (denoted post-BA hp-Ni). Although its SEM images at different magnifications (Figure 5a,b) and XRD pattern (Figure S7 in the Supporting Information) suggested the integrity of the whole three-dimensional hierarchical porous morphology and mainly metallic Ni phase, elemental mapping results (Figure 5c) indicated the presence of Ni and a large amount of O for post-BA hp-Ni. Energy-dispersive X-ray spectroscopy also revealed the increased O content in the post-BA hp-Ni relative to that of fresh hp-Ni (Figure S8 in the Supporting Information), corroborating its surface oxidation during benzyl alcohol oxidation. Additionally, the high-resolution Ni $2p_{3/2}$ XPS spectra for the post-BA hp-Ni electrocatalyst showed an decreased peak at 852.6 eV ascribed to metallic Ni, while an increased peak at 856.0 eV attributed to oxidized Ni species,[22] supporting the partial oxidation of metallic Ni (Figure 5d). This nickel oxidation was further verified by the enhanced peak intensity of high-resolution O 1s XPS spectra (Figure 5e). Collectively, it is most likely that the true catalytic active sites of benzyl alcohol and other related alcohols are the high-valent nickel species.[9,29]

In order to demonstrate that such a strategy of HER coupled with alcohol oxidation is general and can be extended to

DOI: 10.1021/acscatal.7b00876
ACS Catal. 2017, 7, 4564–4570

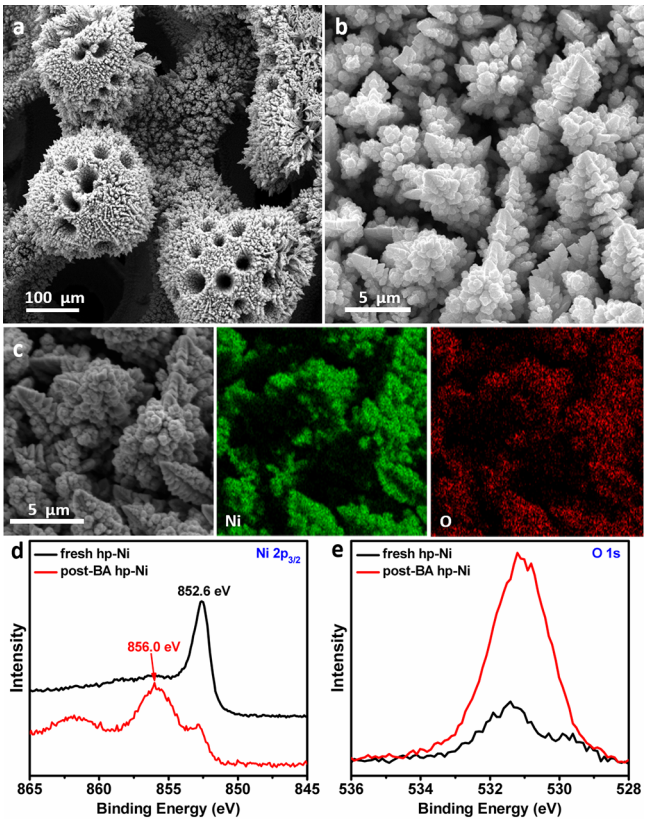

Figure 5. (a, b) SEM images of post-BA hp-Ni at different magnifications. (c) SEM image and the corresponding elemental mapping of post-BA hp-Ni. (d, e) High-resolution XPS spectra of (d) Ni $2p_{3/2}$ and (e) O 1s for the fresh and post-BA hp-Ni electrocatalysts.

upgrading other alcohol compounds, we further evaluated the performance of hp-Ni for the oxidative upgrading of ethanol and 5-hydroxymethylfurfural (HMF), both of which have attracted increasing attention as representative compounds for oxidative alcohol upgrading.[27,29−31,35−37] As depicted in Figure 6, after addition of 10 mM ethanol and HMF, the catalytic onset potentials of hp-Ni both shifted to ∼1.35 V vs RHE and obvious catalytic current density rises were viewed within 1.40 V vs RHE, indicative of alcohol oxidation being more favorable than the OER. The overpotentials to afford a benchmark

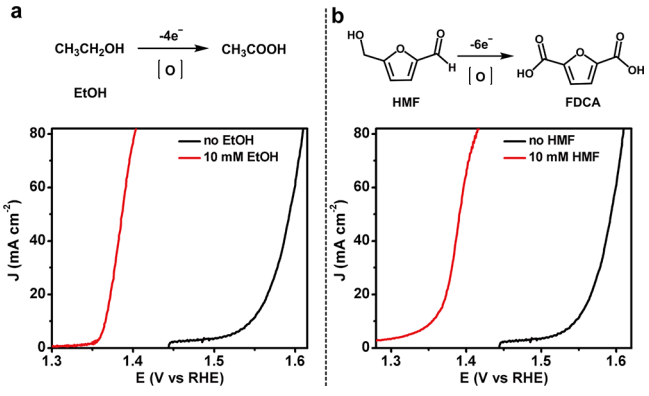

Figure 6. Oxidation of ethanol (a) and HMF (b) to value-added acids and the corresponding linear sweep voltammograms of hp-Ni at 2 mV s^{-1} in 1.0 M KOH in the presence (red) and absence (black) of 10 mM alcohol substrates.

current density (e.g., 50 mA cm^{-2}) for both ethanol and HMF oxidation reactions were at least 200 mV smaller than that of the OER (Figure 6). Chronoamperometry experiments carried out at 1.423 V for the oxidation of ethanol and HMF further demonstrated the almost complete conversion to their corresponding value-added acid products (top of Figure 6). After the theoretical amount of charge was passed, quantitative conversions to the desirable acids were obtained according to the corresponding ^{1}H NMR and HPLC results (Figure S9 in the Supporting Information and Figure 7a).

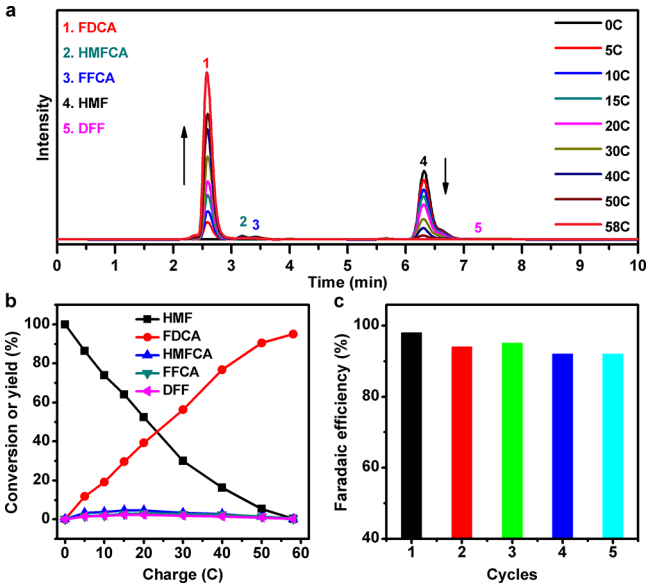

Figure 7. (a) HPLC traces of electrocatalytic HMF oxidation catalyzed by hp-Ni at 1.423 V vs RHE in 10 mL of 1.0 M KOH with 10 mM HMF. (b) Conversion of HMF or yield of the oxidation products during the electrolysis. (c) Faradaic efficiencies of FDCA production using the same hp-Ni catalyst for five successive cycles.

It has been acknowledged that HMF, a dehydration product of C6 carbohydrates from biomass, holds a pivotal place in biomass refinery, as HMF is a platform chemical and can be upgraded to a wide variety of important commodity chemicals (Figure S10 in the Supporting Information), including 2,5-bis(hydroxymethyl)furan, 2,5-dimethylfuran, and 2,5-furandicarboxylic acid (FDCA).[36−39] In particular, FDCA has been suggested as a substitute for terephthalic acid to produce polyamides, polyesters, and polyurethanes.[36−39] Because of the prominent role of HMF as a biomass-derived intermediate compound, we also examined the details of HMF oxidation to FDCA on hp-Ni through a similar chronoamperometry experiment at 1.423 V vs RHE in 10 mL of 1.0 M KOH with 10 mM HMF. In this case, the theoretical amount of ∼58 C charge was calculated for the complete oxidation of HMF to FDCA. As shown in Figure 7b, a high Faradaic efficiency for oxidation of HMF was also expected due to the absence of water oxidation at 1.423 V vs RHE. The obtained HPLC chromatograms (Figure 7a) evidently exhibited a decrease in the peak for HMF and rise of the peak for FDCA over the electrolysis time, intimating the conversion from HMF to FDCA (Figure 7b). After ∼58 C was passed, a Faradaic efficiency of 98% was obtained for the FDCA production. It is known that there are two possible paths for the oxidation of HMF to FDCA (Figure S11 in the Supporting Information):

DOI: 10.1021/acscatal.7b00876
ACS Catal. 2017, 7, 4564−4570

one starts from the oxidation of the aldehyde group of HMF to generate HMFCA, and the other proceeds through the formation of DFF. Subsequently, both routes yield FFCA prior to the eventual formation of FDCA. The relatively higher concentration of HMFCA relative to that of DFF revealed that the hp-Ni-mediated HMF oxidation most likely followed the first-step formation of the HMFCA route, similar to the commonly observed aerobic oxidations.[36] Nevertheless, the DFF route was also included, since the DFF intermediate was still identified via HPLC (Figure 7a). Moreover, the high Faradaic efficiencies (92−98%) of FDCA formation for five successive electrolysis cycles demonstrated the robust stability of hp-Ni for HMF oxidation as well (Figure 7c).

We acknowledge that metallic Ni has been widely used as a cathode catalyst for H_2 production from water electrolysis under alkaline conditions, mainly due to its low cost and excellent catalytic activity.[44] Indeed, our hp-Ni also exhibited great activity for the HER. As shown in Figure S12a in the Supporting Information, the LSV curve of hp-Ni showed a small onset potential and achieved a HER current density of -50 mA cm^{-2} at an overpotential of approximately 219 mV in 1.0 M KOH, comparable to or even better than those of recently reported nonprecious HER catalysts such as β-Mo_2C (>250 mV),[45] η-MoC/C (~220 mV),[46] CoP/CC (>300 mV),[47] and other HER catalysts (Table S1 in the Supporting Information) to reach the same current density. Moreover, hp-Ni exhibited robust long-term stability, as revealed by its stable overpotential of ~230 mV to reach -50 mA cm^{-2} for an 18 h chronopotentiometry experiment (Figure S12b).

Given the outstanding performance of hp-Ni for both alcohol oxidation and H_2 evolution as mentioned earlier, it is highly anticipated that hp-Ni could function as a bifunctional electrocatalyst for simultaneous production of H_2 and organic acid in a two-electrode configuration under alkaline conditions. In order to validate this hypothesis, we chose benzyl alcohol as the organic substrate and an anion exchange membrane was used to separate the two electrodes. As depicted in Figure 8a, our hp-Ni catalyst couple needed a cell voltage of ~1.69 V to afford 10 mA cm^{-2} for water splitting, comparable to or even better than those of previously reported noble-metal-free bifunctional water-splitting catalysts, including NiFe LDH/NF (1.70 V),[48] Ni_5P_4/NF (1.70 V),[49] Ni_3S_2/NF (>1.70 V),[50] and others (Table S2 in the Supporting Information), to reach the same current density. More importantly, upon addition of 10 mM benzyl alcohol, the cell voltages to afford 10, 20, 50, and 100 mA cm^{-2} were noticeably reduced to 1.50, 1.54, 1.60, and 1.66 V, respectively (Figure 8b), substantially smaller than those of pure water electrolysis. In order to quantify the generated H_2 and benzoic acid under this two-electrode setup, a durable electrolysis was performed at a cell voltage of 1.50 V. As exhibited in Figure 8c, the produced H_2 measured by gas chromatography (GC) agreed with the theoretical amounts very well, suggesting a high Faradaic efficiency of ~100% for the HER. Quantifying the resulting liquid products by HPLC also implied a Faradaic efficiency of ~97% for benzoic acid formation. When HMF was selected as the organic substrate, a similarly low energy input and high Faradaic efficiencies for the production of both H_2 and FDCA could also be obtained (Figure S13 in the Supporting Information), demonstrating the versatility of our new-type electrolysis.

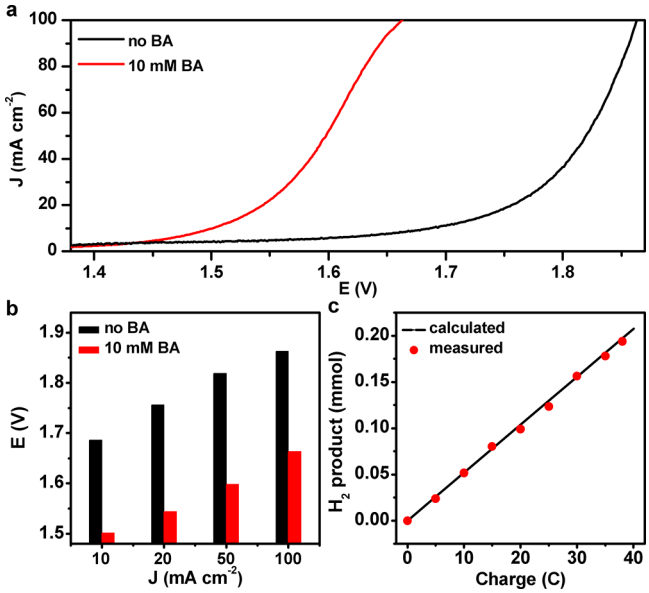

Figure 8. (a) Linear sweep voltammograms and (b) comparison of overpotentials at various current densities utilizing the hp-Ni couple in 1.0 M KOH containing 0 and 10 mM BA. (c) Experimental H_2 quantity compared with the theoretical quantity during the HER catalyzed by the hp-Ni couple.

CONCLUSIONS

In conclusion, we report a general strategy for concurrent H_2 generation and alcohol oxidation catalyzed by the low-cost hp-Ni with nearly unity Faradaic efficiencies. Owing to the more favorable thermodynamics of these alcohol oxidations in comparison to that of the OER on hp-Ni, the electrolyzer voltage to produce benchmark current densities was reduced by ~220 mV in comparison to water-splitting electrolysis. It is even more exciting that value-added products were generated at both electrodes (H_2 at cathode and valuable organic acids at anode). Our strategy provides an alternative approach to avoid the issues of H_2/O_2 mixing and ROS formation during traditional water electrolysis. Given the advantages of inexpensive catalyst, high energy conversion efficiency, great Faradaic efficiency, and ambient reaction conditions (room temperature, atmospheric pressure, and aqueous solution), our new-type electrolysis strategy of cathodic H_2 production coupled with anodic alcohol oxidation should inspire researchers to explore many other oxidative organic upgrading reactions to pair with the HER, maximizing energy conversion efficiency and yielding more valuable products. Finally, the similar onset potentials of hp-Ni for those diverse alcohol substrates with different intrinsic oxidation thermodynamics imply that the catalytic onset is largely determined by the desirable oxidation potential of hp-Ni. Hence, the rational design of catalysts requiring lower oxidation potential is anticipated to lead to electrocatalytic organic oxidation at even smaller voltage input. Further studies along this line are underway.

ASSOCIATED CONTENT

Supporting Information

The Supporting Information is available free of charge on the ACS Publications website at DOI: 10.1021/acscatal.7b00876.

DOI: 10.1021/acscatal.7b00876
ACS Catal. 2017, 7, 4564−4570

Additional figures, electrochemical plots, tables, XRD, XPS, SEM, and NMR data, and HPLC chromatograms (PDF)

AUTHOR INFORMATION

Corresponding Author

*E-mail for Y.S.: yujie.sun@usu.edu.

ORCID

Bo You: 0000-0003-1849-0418

Yujie Sun: 0000-0002-4122-6255

Author Contributions

§B.Y., X.L., and X.L. contributed equally.

Notes

The authors declare no competing financial interest.

ACKNOWLEDGMENTS

We acknowledge the support of the National Science Foundation (CHE-1653978) and the Microscopy Core Facility at Utah State University. X.L. acknowledges financial support from the Chinese Academy of Sciences Funded Overseas Study Program and the Qinghai Institute of Salt Lakes, Chinese Academy of Sciences. The NMR measurements were conducted on a NMR spectrometer supported by an NSF MRI Award (CHE-1429195).

REFERENCES

(1) Shi, Y.; Zhang, B. *Chem. Soc. Rev.* **2016**, *45*, 1529−1541.
(2) You, B.; Sun, Y. *ChemPlusChem* **2016**, *81*, 1045−1055.
(3) Zheng, Y.; Jiao, Y.; Jaroniec, M.; Qiao, S. Z. *Angew. Chem., Int. Ed.* **2015**, *54*, 52−65.
(4) Nichols, E. M.; Gallagher, J. J.; Liu, C.; Su, Y.; Resasco, J.; Yu, Sun, Y. Y.; Yang, P.; Chang, M. C. Y.; Chang, C. J. *Proc. Natl. Acad. Sci. U. S. A.* **2015**, *112*, 11461−11466.
(5) Kang, D.; Kim, T. W.; Kubota, S. R.; Cardiel, A. C.; Cha, H. G.; Choi, K.-S. *Chem. Rev.* **2015**, *115*, 12839−12887.
(6) Thoi, V. S.; Sun, Y.; Long, J. R.; Chang, C. J. *Chem. Soc. Rev.* **2013**, *42*, 2388−2400.
(7) Benck, J. D.; Hellstern, T. R.; Kibsgaard, J.; Chakthranont, P.; Jaramillo, T. F. *ACS Catal.* **2014**, *4*, 3957−3971.
(8) Zeng, M.; Li, Y. *J. Mater. Chem. A* **2015**, *3*, 14942−14962.
(9) Smith, R. D. L.; Berlinguette, C. P. *J. Am. Chem. Soc.* **2016**, *138*, 1561−1567.
(10) Diaz-Morales, O.; Ledezma-Yanez, I.; Koper, M. T. M.; Calle-Vallejo, F. *ACS Catal.* **2015**, *5*, 5380−5387.
(11) Burke, M. S.; Enman, L. J.; Batchellor, A.; Zou, S.; Boettcher, S. W. *Chem. Mater.* **2015**, *27*, 7549−7558.
(12) Batchellor, A. S.; Boettcher, S. W. *ACS Catal.* **2015**, *5*, 6680−6689.
(13) Jiang, N.; You, B.; Sheng, M.; Sun, Y. *Angew. Chem., Int. Ed.* **2015**, *54*, 6251−6254.
(14) Anantharaj, S.; Ede, S. R.; Sakthikumar, K.; Karthick, K.; Mishra, S.; Kundu, S. *ACS Catal.* **2016**, *6*, 8069−8097.
(15) Yan, Y.; Xia, B. Y.; Zhao, B.; Wang, X. *J. Mater. Chem. A* **2016**, *4*, 17587−17603.
(16) Jamesh, M. I. *J. Power Sources* **2016**, *333*, 213−236.
(17) Lai, J.; Li, S.; Wu, F.; Saqib, M.; Luque, R.; Xu, G. *Energy Environ. Sci.* **2016**, *9*, 1210−1214.
(18) Zhang, J.; Dai, L. *Angew. Chem., Int. Ed.* **2016**, *55*, 13296−13300.
(19) Wang, H.; Min, S.; Ma, C.; Liu, Z.; Zhang, W.; Wang, Q.; Li, D.; Li, Y.; Turner, S.; Han, Y.; Zhu, H.; Abou-hamad, E.; Hedhili, N.; Pan, J.; Yu, W.; Huang, K. W.; Li, L. J.; Yuan, J.; Antonietti, M.; Wu, T. *Nat. Commun.* **2017**, *8*, 13592.
(20) Wang, H.; Lee, H.-W.; Deng, Y.; Lu, Z.; Hsu, P.-C.; Liu, Y.; Lin, D.; Cui, Y. *Nat. Commun.* **2015**, *6*, 7261.
(21) Chen, Y. X.; Lavacchi, A.; Miller, H. A.; Bevilacqua, M.; Filippi, J.; Innocenti, M.; Marchionni, A.; Oberhauser, W.; Wang, L.; Vizza, F. *Nat. Commun.* **2014**, *5*, 4036.
(22) You, B.; Jiang, N.; Sheng, M.; Bhushan, M. W.; Sun, Y. *ACS Catal.* **2016**, *6*, 714−721.
(23) Symes, M. D.; Cronin, L. *Nat. Chem.* **2013**, *5*, 403−409.
(24) Rausch, B.; Symes, M. D.; Chisholm, G.; Cronin, L. *Science* **2014**, *345*, 1326−1330.
(25) Rausch, B.; Symes, M. D.; Cronin, L. *J. Am. Chem. Soc.* **2013**, *135*, 13656−13659.
(26) Bloor, L. G.; Solarska, R.; Bienkowski, K.; Kulesza, P. J.; Augustynski, J.; Symes, M. D.; Cronin, L. *J. Am. Chem. Soc.* **2016**, *138*, 6707−6710.
(27) Kasap, H.; Caputo, C. A.; Martindale, B. C. M.; Godin, R.; Lau, V. W.; Lotsch, B. V.; Durrant, J. R.; Reisner, E. *J. Am. Chem. Soc.* **2016**, *138*, 9183−9192.
(28) Jiang, N.; Liu, X.; Dong, J.; You, B.; Liu, X.; Sun, Y. *ChemNanoMat.* **2017**, DOI: 10.1002/cnma.201700076.
(29) You, B.; Jiang, N.; Liu, X.; Sun, Y. *Angew. Chem., Int. Ed.* **2016**, *55*, 9913−9917.
(30) Jiang, N.; You, B.; Boonstra, R.; Rodriguez, I. M.; Sun, Y. *ACS Energy Lett.* **2016**, *1*, 386−390.
(31) You, B.; Liu, X.; Jiang, N.; Sun, Y. *J. Am. Chem. Soc.* **2016**, *138*, 13639−13646.
(32) McCrory, C. C. L.; Jung, S.; Ferrer, I. M.; Chatman, S. M.; Peters, J. C.; Jaramillo, T. F. *J. Am. Chem. Soc.* **2015**, *137*, 4347−4357.
(33) You, B.; Sun, Y. *Adv. Energy Mater.* **2016**, *6*, 1502333.
(34) You, B.; Jiang, N.; Sheng, M.; Gul, S.; Yano, J.; Sun, Y. *Chem. Mater.* **2015**, *27*, 7636−7642.
(35) Badalyan, A.; Stahl, S. S. *Nature* **2016**, *535*, 406−410.
(36) Zhang, Z.; Deng, K. *ACS Catal.* **2015**, *5*, 6529−6544.
(37) Zakrzewska, M. E.; Bogel-Lukasik, E.; Bogel-Lukasik, R. *Chem. Rev.* **2011**, *111*, 397−417.
(38) Lv, G.; Wang, H.; Yang, Y.; Deng, T.; Chen, C.; Zhu, Y.; Hou, X. *ACS Catal.* **2015**, *5*, 5636−5646.
(39) Cha, H. G.; Choi, K.-S. *Nat. Chem.* **2015**, *7*, 328−333.
(40) Ma, T. Y.; Dai, S.; Jaroniec, M.; Qiao, S. Z. *J. Am. Chem. Soc.* **2014**, *136*, 13925−13931.
(41) You, B.; Jiang, N.; Sheng, M.; Drisdell, W. S.; Yano, J.; Sun, Y. *ACS Catal.* **2015**, *5*, 7068−7076.
(42) You, B.; Kang, F.; Yin, P.; Zhang, Q. *Carbon* **2016**, *103*, 9−15.
(43) You, B.; Yin, P.; An, L. *Small* **2014**, *10*, 4352−4361.
(44) Gong, M.; Zhou, W.; Tsai, M.-C.; Zhou, J.; Guan, M.; Lin, M.-C.; Zhang, B.; Hu, Y.; Wang, D.-Y.; Yang, J.; Pennycook, S. J.; Hwang, B.-J.; Dai, H. *Nat. Commun.* **2014**, *5*, 4695.
(45) Wan, C.; Regmi, Y. N.; Leonard, B. M. *Angew. Chem., Int. Ed.* **2014**, *53*, 6407−6410.
(46) Wu, H. B.; Xia, B. Y.; Yu, L.; Yu, X. Y.; Lou, X. W. *Nat. Commun.* **2015**, *6*, 6512.
(47) Tian, J.; Liu, Q.; Asiri, A. M.; Sun, X. *J. Am. Chem. Soc.* **2014**, *136*, 7587−7590.
(48) Luo, J.; Im, J.-H.; Mayer, M. T.; Schreier, M.; Nazeeruddin, M. K.; Park, N.-G.; Tilley, S. D.; Fan, H. J.; Grätzel, M. *Science* **2014**, *345*, 1593−1596.
(49) Ledendecker, M.; Krick Calderon, S.; Papp, C.; Steinruck, H.-P.; Antonietti, M.; Shalom, M. *Angew. Chem., Int. Ed.* **2015**, *54*, 12361−12365.
(50) Feng, L.-L.; Yu, G.; Wu, Y.; Li, G.-D.; Li, H.; Sun, Y.; Asefa, T.; Chen, W.; Zou, X. *J. Am. Chem. Soc.* **2015**, *137*, 14023−14026.

DOI: 10.1021/acscatal.7b00876
ACS Catal. 2017, 7, 4564−4570